VARIABILITY AND FORCING OF CLIMATE PARAMETERS ON THE GREENLAND ICE SHEET: GREENLAND CLIMATE NETWORK (GC-NET)

Konrad Steffen, Nicolas Cullen Russell Huff, Sandy Starkweather,
Todd Albert, Molly McAllister
University of Colorado at Boulder
Cooperative Institute for Research in Environmental Sciences
Division of Cryospheric and Polar Processes
Campus Box 216, Boulder CO 80309

NAG5-10857
Annual Progress Report
to
National Aeronautics and Space Administration
March 2003

JAR3 AUTOMATIC WEATHER STATION IN THE ABLATION REGION (JUNE 2003)

TABLE OF CONTENTS

1. ACTIVITIES

1.1 Summary of Highlights

Greenland Climate network (GC-Net)

- Fourteen AWS sites have been visited and serviced in spring 2003: ETH/CU, CP1, JAR1, JAR2, JAR3, DYE-2, Saddle, NASA-SE, Summit, Petermann, Humboldt, Tunu-N, NASA-E, NASA-U (Fig. 1.1).
- One new AWS was installed at the equilibrium line altitude of Petermann Gletscher at 80° 05' 02" N, 58° 04' 02" W, 965 m in Northwestern Greenland.
- Ground-penetrating radar profiles were made at Tunu-N and NASA-U to study the ice layer and accumulation variability in a 100 x 100 m region.
- Quality control (QC) procedures have been refined and applied to all data, including data collected during the 2002 field campaign.
- The satellite transmitted AWS raw data can now be processed and quality controlled with IDL programs on Window 2000 computers.
- Results supported by this grant have been published in nine peer-reviewed publications in 2003.

Applications and Results

- The mean annual temperature at Swiss Camp is -12.4° C over the ten-year time period 1993-2002.
- The largest monthly mean net radiation At Swiss Camp was found in summer 1995 (> 40 W m^{-2}) over the ten-year time period 1993-2002, coincident with the time period with minimum.
- The ten-year annual mean net radiation at Swiss Camp is –13.9 W m^{-2}, and for the winter month November to February a negative mean flux density of –26.4 W m^{-2} was recorded.
- At the top of the ice sheet (Summit) an annual increase of temperature of 0.03 °C/yr has occurred during this time but is not statistically significant ($p > 0.05$). Winter temperatures (DJF) have increased by 0.21 °C/yr but this trend is also not statistically significant. Interestingly, over the period 1987-2002 summer temperatures (JJA) have decreased at Summit by 0.16 °C/yr, and is significant at the $p < 0.06$ level.
- The 2003 melt season was the fifth largest melt season in terms of total melt and melt extent in the passive microwave record which is continuous since 1979.
- Due to very low precipitation rates on the western flank of the ice sheet in 2003, the albedo during the peak of the melt season was unusually low resulting in a highly intense melt season. As a result nearly 1.3 m of ice was melted at the Swiss camp station located near the ELA.
- Cyclone intensity has shown a stronger correlation to total melt than cyclone frequency on the Greenland ice sheet for all regions.
- Summit, Greenland is an extreme environment for the performance of any satellite data product. Atmospheric water vapor is very low, surface inversions are common and polar night conditions prevail for half of the year. The MODIS cloud mask MOD_35 performs well in this environment in spite of having been optimized for lower latitudes and implementing coarse domain-based thresholds.

1.2 Logistic Summary

Date	Location	Work
April 2003		
14	Scotia-SFJ	4 team member and cargo on C-130 (Box, Cullen, Huff, McAllister)
15	SFJ-SWC	Box, Cullen, Huff, McAllister Flight with Twin Otter open Swiss Camp
16	SFJ-SWC-CP1	2nd cargo flight and service of CP1 AWS
24	CPH-SFJ-Ilulissat	Air Greenland flight: Steffen and Zwally
25	Ilulissat-SWC	Air Alpha helicopter flight to camp (Steffen and Zwally)
26	SWC	Download AWS data from 3 towers at SWC
27	JAR	Download Jar2, SMS2, SMS3 AWS data
29	SWC-SFJ	Twin Otter flight – Steffen, Huff and Cullen are leaving for Petermann Glacier project
May 2003		
6	SFJ-SWC-SFJ	Pull-out Swiss Camp: Zwally, Box, McAllister
8	SFJ-CPH	Zwally leaves with Air Greenland
9-13	southern travers	AWS maintenance (Box, McAllister)
17	SFJ-Scotia	Air National C-130 flight back to US (Box, McAllister)
30	Thule - NASA E	AWS maintenance at NASA-E with Twin Otter, Cullen, Stewart staying two nights
30	NASA E - Tunu N	AWS maintenance at Tunu-N, Steffen and Huff staying 2 nights
30	Tunu N –DMH	Plane goes to east coast
31	Tunu N	GPR profiles for ice layer and accumulation study
June 2003		
1	DMH - Tunu N	pick-up Steffen and Huff
1	Tunu N – NASA E	pick-up Cullen and Stewart
1	NASA E – Summit	Refuel Twin Otter and download Summit AWS
1	Summit – NASA U	AWS maintenance and 3 m snow pit, plane leaves for west coast, Steffen, Huff, Cullen, Stewart, and Saskia staying over night
2	NASA U	GPR profiles for ice layer and accumulation study
3	NASA U – Ilulissat	transit for helicopter flight
3	Ilulissat – JAR3	Air Greenland helicopter flight to JAR3, drilling and maintenance
3	Ilulissat – SFJ	Twin Otter flight with cargo and 5 pax
5	SFJ-CPH	Air Greenland flight Steffen
6	SFJ-Scotia	C130 flight back to US, Huff, Cullen

1.3 Personal

Name	Institution	Arr.	Dep.
Jason Box	Ohio State University	4/14	5/17
Nicolas Cullen	CU-Boulder	4/14	6/6
Molly McAllister	CU-Boulder	4/14	5/17
Russ Huff	CU-Boulder	4/14	6/6
Konrad Steffen	CU-Boulder	4/24	6/5
Jay Zwally	GSFC-NASA	4/24	5/6

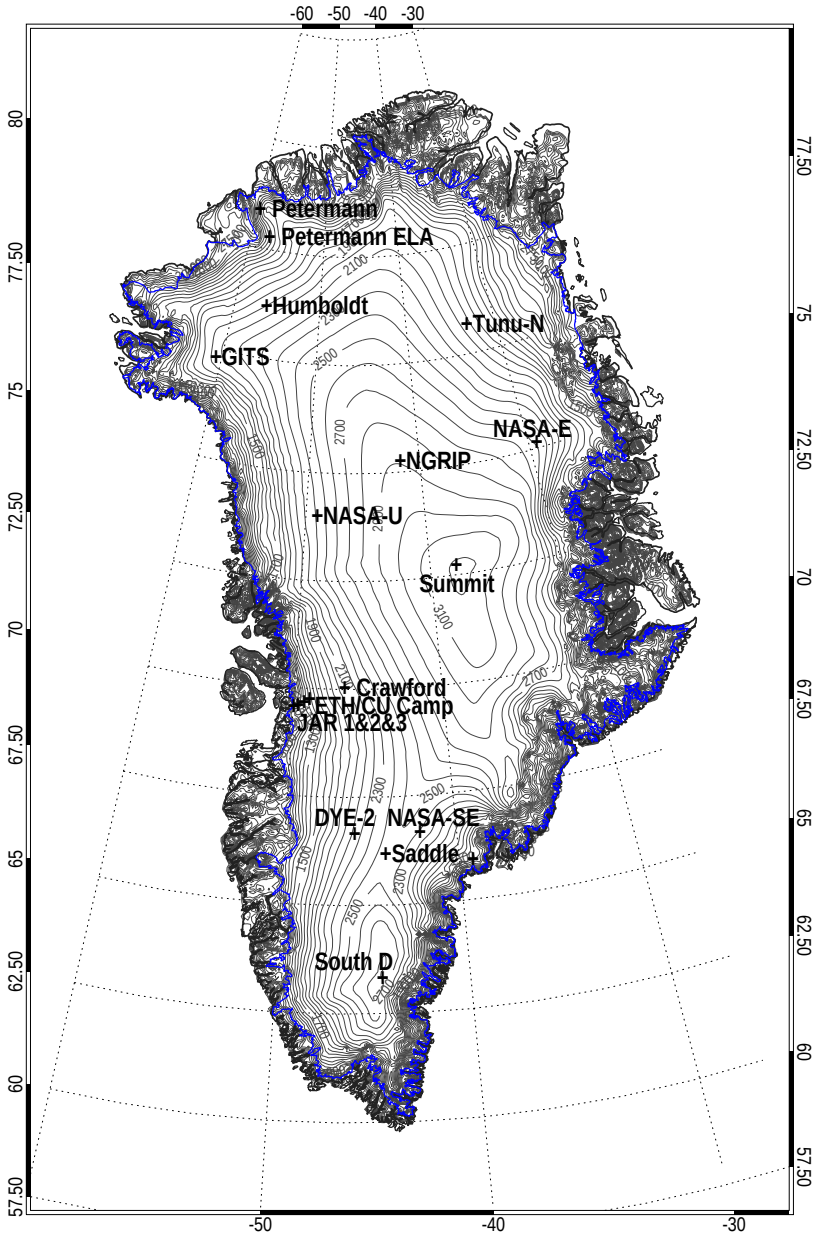

Figure 1.1: Greenland Climate Network (GC-Net) automatic weather stations as of summer 2003.

2. GREENLAND CLIMATE NETWORK (GC-NET)

2.1 Overview

The GC-Net currently consists of 18 automatic weather stations and four smart stakes distributed over the entire Greenland ice sheet (Figure 1.1). Four stations are located along the crest of the ice sheet (2500 to 3200 m elevation range) in a north-south direction, Eeight stations are located close to the 2000 m contour line (1830 m to 2500 m), and four stations are positioned in the ablation region (50 m to 800 m), and two stations are located at the equilibrium line altitude at the west coast and in the north.). The smart stakes were introduced in spring 2001 to measure the climate in the ablation region in the Jakobshavn area (SMS1-5), and one on the floating tongue of Petermann Gletscher.

The GC-Net was established in spring 1995 with the intention of monitoring climatological and glaciological parameters at various locations on the ice sheet over a time period of at least 10 years. The first AWS was installed in 1990 at the Swiss Camp, followed by four AWS in 1995, four in 1996, five in 1997, another four in 1999, one in 2002 and the latest one in 2003. Our objectives for the Greenland weather station (AWS) network are to measure daily, annual and interannual variability in accumulation rate, surface climatology and surface energy balance at selected locations on the ice sheet, and to measure near-surface snow density at the AWS locations for the assessment of snow densification, accumulation, and metamorphosis.

In addition to providing climatological and glaciological observations from the field, further application of the GC-Net data include: the study of the ice sheet melt extent [*Abdalati and Steffen*, 2001]; estimates of the ice sheet sublimation rate [*Box and Steffen*, 2001]; reconstruction of long-term air temperature time series [*Shuman at al.*, 2001], assessment of surface climate [*Steffen and Box*, 2001], and the interpretation of satellite-derived melt features of the ice sheet [*Nghiem et al.*, 2001]. Potential applications for the use of the GC-Net data are: comparison of in-situ and satellite-derived surface parameters, operational weather forecast; validation of climate models; and logistic support for ice camps and Thule AFB.

2.2 Data Processing

Currently, a total of 630 parameters are transmitted every hour, and until a site is revisited, transmitted data are used. All the AWS sites are revisited within 2-3 years depending on logistics and accumulation. Statistical procedures are applied to the GC-Net data in effort to improve data quality. These include (a) the rejection of impossible values, and (b) using a gradient threshold comparing the measurement with the next sequential hourly value. A moving sample interval scans the time series to identify and reject data beyond a variance threshold for a given sample size. In some cases, a spectrum of window sizes is employed to reject outliers due to occasional data scrambling by transmission errors. In general, the data that are rejected by these filters represent a minor fraction of the data volume. Once a station is re-visited, continuous data are retrieved to replace the transmitted data.

Data processing during 2003 was accomplished in five phases. During January all transmitted data for 2002 was processed and year end quality control was completed. During the field season, data from the Petermann AWS and SMS was analyzed in the field using newly developed routines for field data ingest designed to run on portable field computers. This process insures that all necessary field measurements and notes are taken before leaving the site as well as identifying instruments that may have experienced intermittent failure since the last visit. We intend to complete field data ingest and quality control on site at as many of the stations visited as possible in 2004. In July, 2003 all field collected data was assimilated and quality checked. In November, all transmitted data was processed prior to the Fall American Geophysical Union meeting. Finally, in January, 2004 all transmitted data from 2003 was processed and year end quality con-

trol was completed. It was noted that files containing the continuous data records for each station had not been updated since 2001. These files have now been updated through 2003. A secondary quality check on all of the surface height data and subsequent reprocessing significantly increased the quality of these data as well.

The suite of IDL routines for processing the AWS data on a PC using standard windows graphical user interfaces has continued to grow. The primary program (Figure 2.1) for calibrating and cleaning the field collected data has been enhanced in several areas. First, a new data visualization routine has been incorporated allowing users to efficiently view all GC-NET data including newly field collected data files, AWS and SMS files, and pre and post quality controlled data file formats. Figure 2.2 illustrates the user interface. Features include a zooming window, thumbnail selection of all available data channels, signal overlays, printing and export. Secondly a new tool for visually identifying and filtering spurious data has been developed. This tool replaces a tedious trial and error approach that involved modifying the quality control program code each time new data was acquired. The tool has drastically reduced the time required for quality control as well as increased the quality of the final product. The tool is depicted in Figure 2.3. The programs for processing field collected data have also continued to evolve to the point where they are ready to be used while in the field further increasing the quality of the final data product as well as identifying potential hardware failures before leaving the station. The user interfaces for the GOES and ARGOS field data ingest routines are depicted in Figures 2.4 and 2.5.

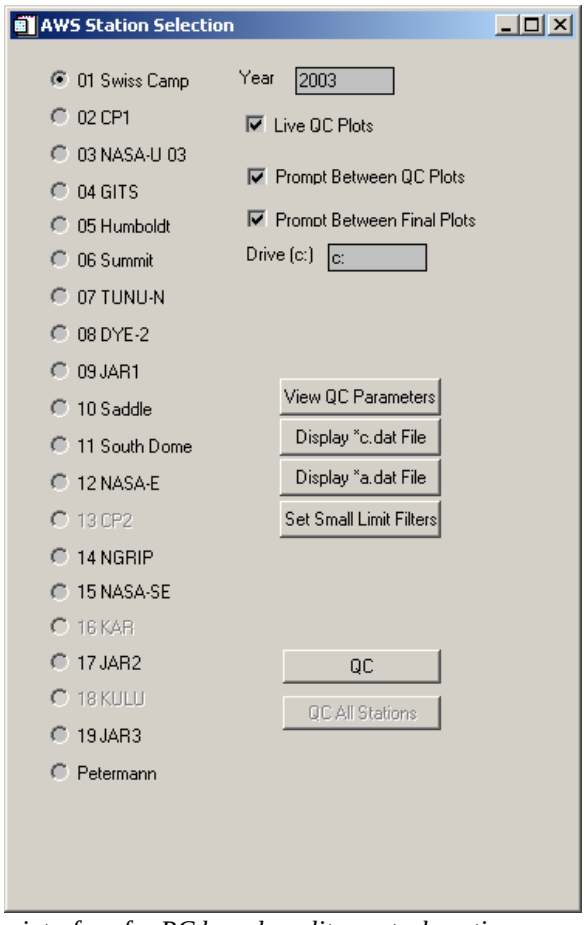

Figure 2.1: Graphical user interface for PC based quality control routine.

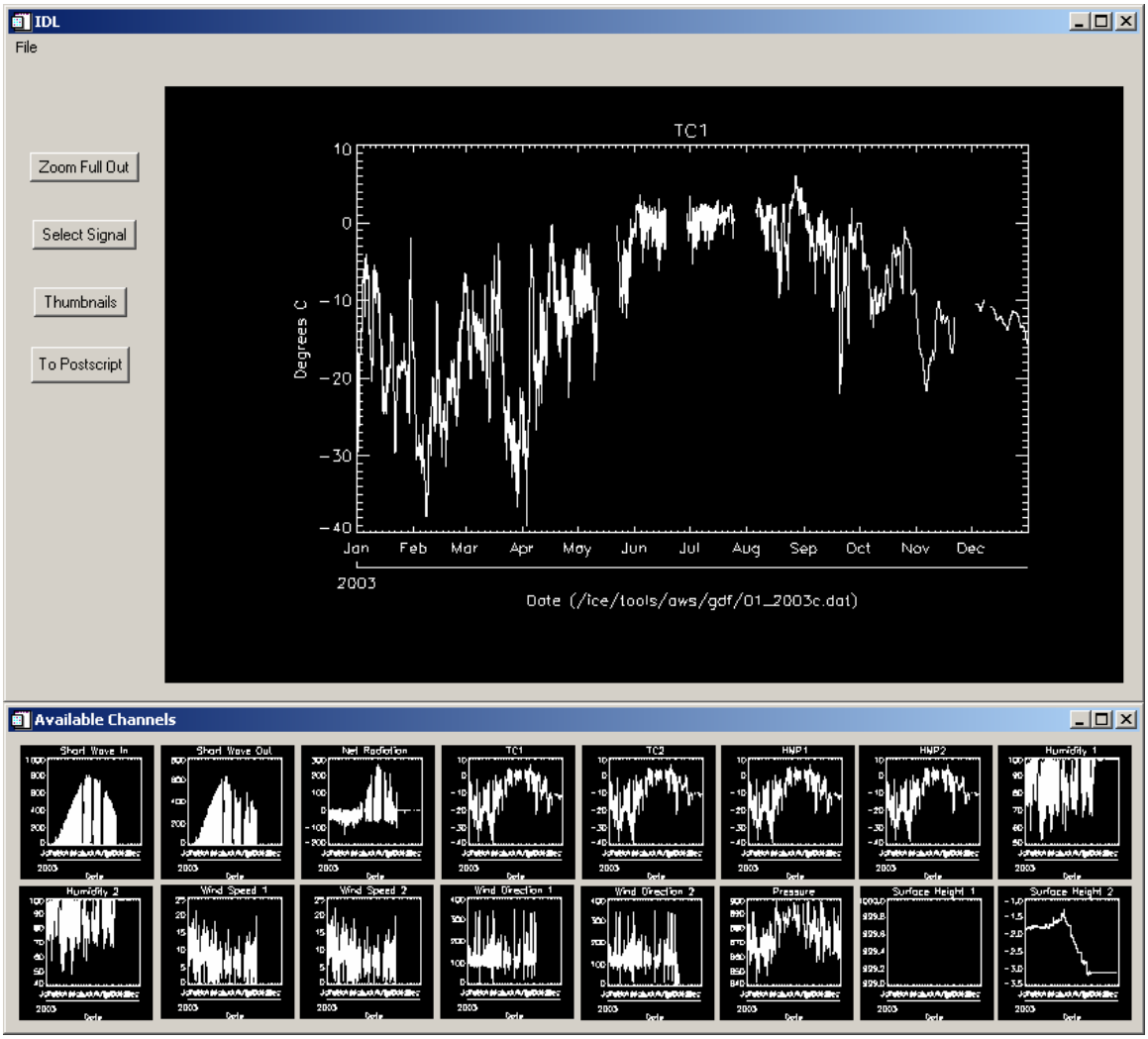

Figure 2.2: Graphical user interface and signal selection menu for GC-NET visualization tool.

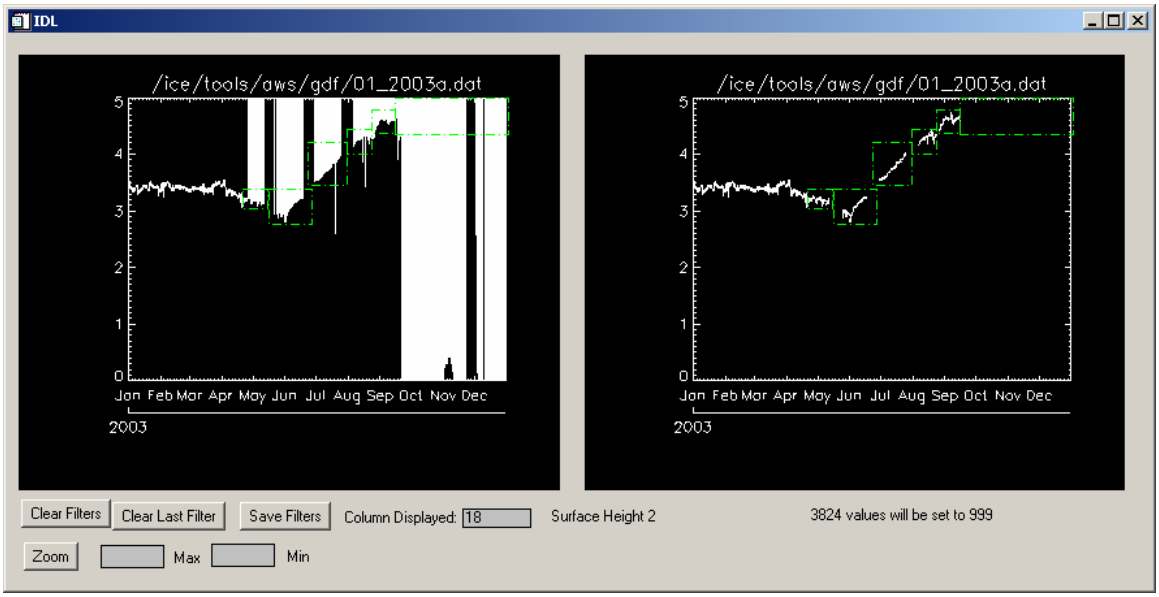

Figure 2.3: Visual tool for data cleaning.

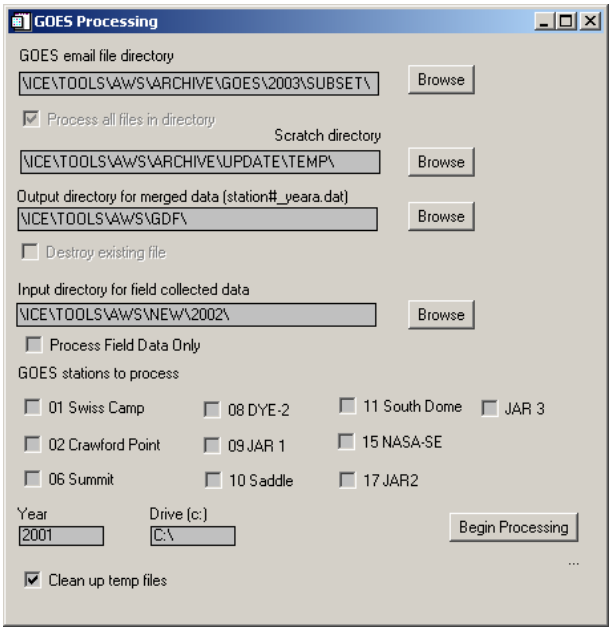

Figure 2.4: Field data ingest routine for GOES stations.

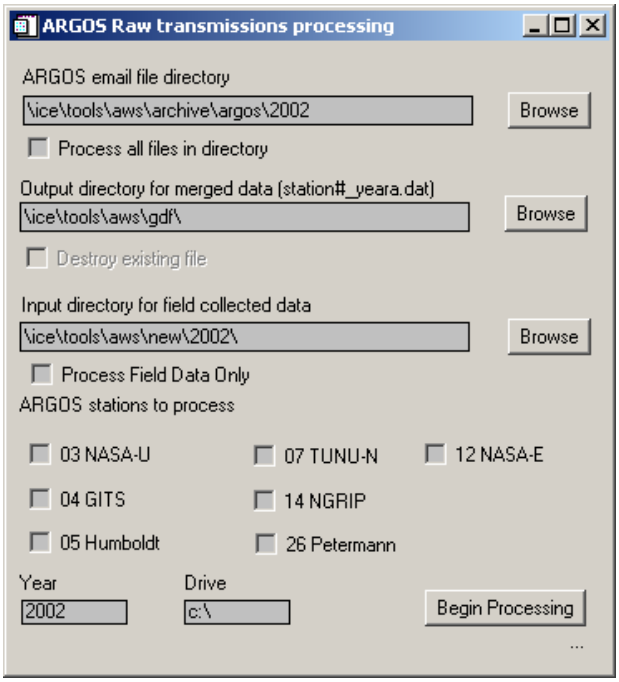

Figure 2.5: Field data ingest routine for ARGOS stations.

2.4 GC-Net Citation List

This list represents publications that made use of Greenland Climate Network (GC-Net) data.

Abdalati, W. and K. Steffen, Greenland ice sheet melt extent: 1979-1999, *J. Geophys. Res*., 106(D24), 33,983-33,989, 2001.

Box, J. E., Surface Water Vapor Exchange on the Greenland Ice Sheet Derived from Automated Weather Station Data, PhD Thesis, Department of Geography, University of Colorado, Boulder, CO, Cooperative Institute for Research in Environmental Sciences, 190 pp, 2001.

Box, J.E. and K. Steffen, Sublimation on the Greenland ice sheet from automated weather station observations, *J. Geophys. Res*., 106(D24), 33,965-33,982, 2001.

Bromwhich, D., J. Cassano, T. Klein, G. Heinemann, K. Hines, K. Steffen and J. Box, Mesoscale modeling of katabatic winds over Greenland with Polar MM5, *Mon. Weather Review*, 129, 2290-2309, 2001.

Cassano, J.J., J.E. Box, D.H. Bromwich, L. Li, and K. Steffen, Evaluation of Polar MM5 simulations of Greenland's atmospheric circulation, *J. Geophys. Res*., 106(D24), 33,867-33,890, 2001.

Cullen, N., and K. Steffen, Unstable near-surface boundary conditions in summer on top of the Greenland ice sheet., *Geophys. Res. Lett*., 28(23), 4491-4494, 2001.

Davis, C.H. and D.M. Segura, An algorithm for time-series analysis of ice sheet surface elevations from satellite altimetry, *IEEE Transactions on Geoscience & Remote Sensing*, 39(1), 202-206, 2001.

Dassau, T.M., A. Sumer, S. Koeniger, P. Shepson, J. Yang, R. Honrath, N. Culen, K. Steffen, Investigation of the role of the snowpack on atmospheric formaldehyde chemistry at Summit, Greenland, J. Geophys. Res., 107(D19), ACH 9.1-14, 36, 2595-2608, 2002.

Hanna, E. and P. Valdes, Validation of ECMWF (re)analysis surface climate data, 1979-1998, for Greenland and implications for mass balance modeling of the Ice Sheet, *Intern. J. Clim.*, 21, 171-195, 2001.

Helmig, D, J. Boulter, D. David, J. Birk, N. Cullen, K. Steffen, B. Johsnon, S. Oltmans, Ozone and meteorological boundary-layer conditions at Summit, Greenland, *Atm. Environm*., 36, 2595-2608, 2002.

Honrath, R.E. Y.Y. Lu, M.C. Peterson, J.E. Dibb, M.A. Arseault, N.J. Cullen, and K. Steffen. vertical fluxes of NOx, HONO, and HNO3 above the snowpack at Summit, Greenland. *Atm. Environm*, 36, 2629-2640, 2002.

Klein, T., G. Heinemann, D. H. Bromwich, J. J. Cassano and K. M. Hines, Mesoscale modeling of katabatic winds over Greenland and comparisons with AWS and aircraft data, *J. Met. Atmos. Phys*., 8(1/2), 115-132, 2001.

Klein, T., G. Heinemann, Simulations of the katabatic wind over the Greenland ice sheet with a 3D model for one winter month and two spring months, Report of the DAAD/NSF project 315-PP, 1999.

Mosley-Thompson, E., J.R. McConnell, R.C. Bales, Z. Li, P.-N. Lin, K. Steffen, L.G. Thompson, R. Edwards, D. Bathke, Local to regional-scale variability of annual net accumulation on the Greenland ice sheet from PARCA cores, *J. Geophys. Res*., 106 (D24), 33,839-33852, 2001.

Murphy, B. F., I. Marsiat and P. Valdes, Simulated atmospheric contributions to the surface mass balance of Greenland. *J. Geophys. Res*., 106, submitted, 2001.

Nghiem, S.V., K. Steffen, R. Kwok, and W.Y. Tsai, Diurnal variations of melt regions on the Greenland ice sheet, *J. Glaciol*., 47(159), 539-547, 2001.

Nolin, A. and J. Stroeve The Changing Albedo of the Greenland Ice Sheet: Implications for Climate Change, Annals of Glaciology, 25, 51-57, 1997.

Serreze, M., J. Key, J. Box, J. Maslanik, and K. Steffen, A new monthly climatology of global radiation for the Arctic and comparison with NCEP-NCAR reanalysis and ISCCP-C2 field, *J. Climate*, 11, 121-136, 1998.

Shuman, C., K. Steffen, J. Box, and C. Stearn, A dozen years of temperature observations at the Summit: Central Greenland automatic weather stations 1987-1999, *J. Appl. Meteorol*., 40(4),741-752, 2001.

Smith, L.C., Y. Sheng, R.R. Foster, K. Steffen, K.E. Frey, and D.E. Alsdorf, Melting of small Arctic ice caps observed from ERS scatterometer time series, Geophys. Res. Lett., 30(20), CRY 2-14, 2003.

Steffen, K., and J.E. Box, Surface climatology of the Greenland ice sheet: Greenland climate network 1995-1999, *J. Geophys. Res*., 106(D24), 33,951-33,964, 2001.

Steffen, K., W. Abdalati, and I. Serjal, Hoar development on the Greenland ice sheet, *J. of Glaciology*, 45(148), 63-68, 1999.

Steffen, K., J. E. Box and W. Abdalati, Greenland climate network: GC-Net, *CRREL, 98-103* pp., 1996.

Stroeve, J., Assessment of Greenland Albedo Variability from the AVHRR Polar Pathfinder Data Set, *J. Geophys. Res*., 106(D24), 33,989-34,006, 2001.

Stroeve, J., and A. Nolin, 1997. The changing albedo of the Greenland ice sheet: implications for climate modeling, *Ann. of Glaciol*., 25, 51-57.

Stroeve, J, J. E. Box, J. Maslanik, J. Key, C. Fowler, Intercomparison between in situ and AVHRR Polar Pathfinder-derived surface albedo over Greenland, *Remote Sensing of the Environment*, 75(3), 360-374, 2001.

Thomas, R., and PARCA instigators, Program for Arctic Regional Climate Assessment (PARCA): Goals, key findings, and future directions, *J. Geophys. Res*., 106(D24), 33,691-33706, 2001.

Thomas, R.H., W. Abdalati, E. Frederick, W.B. Krabill, S. Manizade, and K. Steffen, Investigation of surface melting and dynamic thinning on Jakobshavn Isbrea, Greenland, J. Glaciol., 49(165), 231-239, 2003.

Zwally, H.J. W. Abdalati, T. Herring, K. Larsen, J. Saba, and K. Steffen. Surface melt-induced acceleration of Greenland ice-sheet flow, *Science*, 297, 218-222, 2002.

3. APPLICATIONS AND RESULTS

3.1 Temperature and Radiation Climatology at Swiss Camp (1993-2002)

The mean annual temperature at Swiss Camp is -12.4° C over the ten-year time period 1993-2002. The coldest monthly mean temperatures are found in February with values as low as -27.5° C and the warmest summer month is generally July with values slightly above freezing (Figure 3.1).

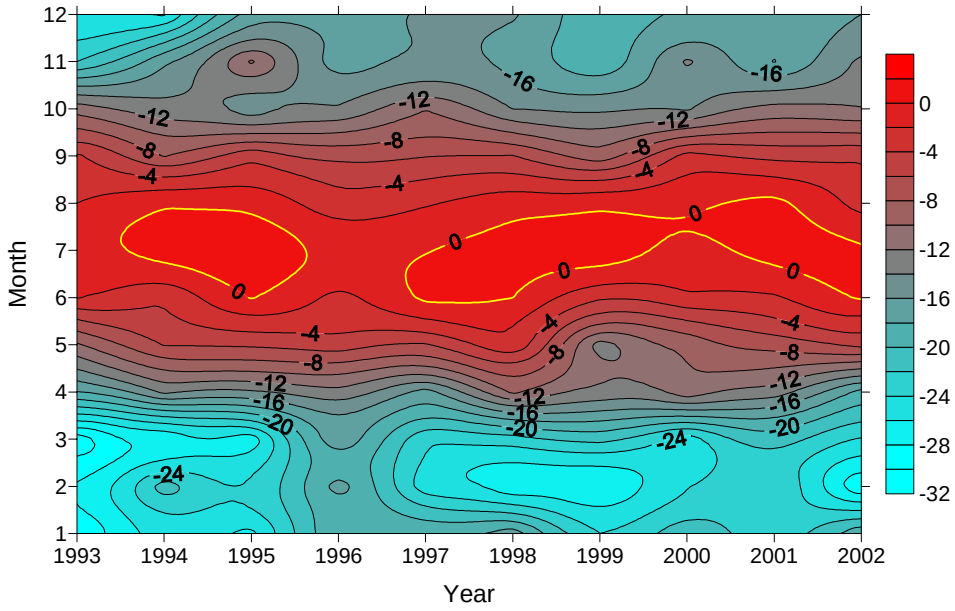

.3.1: ***Interannual variability of monthly mean air temperatures (1993 – 2002) at the Swiss Camp ETH/CU, located at the equilibrium line altitude on the western slope of the Greenland ice sheet.***

Radiation has been monitored continuously at Swiss Camp since 1993. The time series of mean monthly net radiation values is plotted in Figure 3.2 for the 1993 – 2002 period.

The largest monthly mean net radiation values are found in summer 1995 (> 40 W m^{-2}), coincident with the time period when a minimum in insolation occurred (not shown). During the same summer, mean monthly air temperatures (Figure 3.1) above 0 °C were common during the month of July, indicating a strong albedo-feedback mechanism for this region at the ELA. Most of the annual snow cover melted during summer 1995, reducing the monthly albedo value to 0.6. Only the summer of 2001 had albedo values that low. Surface melting was further enhanced during the summer of 1995 due to above average cloud amount (not shown here), and hence increasing long-wave radiation.

It is worth discussing the three anomalous years 1995, 1998, and 2001. Figure 3.2 shows the monthly net radiation values for the entire time period; each summer is characterized by a positive net radiation flux, which is indicative of the length of the melting period. Maximum mean values of 350 W m^{-2} (1995) demonstrate the negative albedo feedback effect of the low ice albedo. The length of the melting period in 1995, however, is similar to other years. The 4-month period of positive net radiation in 1998, 2000 and 2001 coincides with the warmest years on record for the western part of the ice sheet.

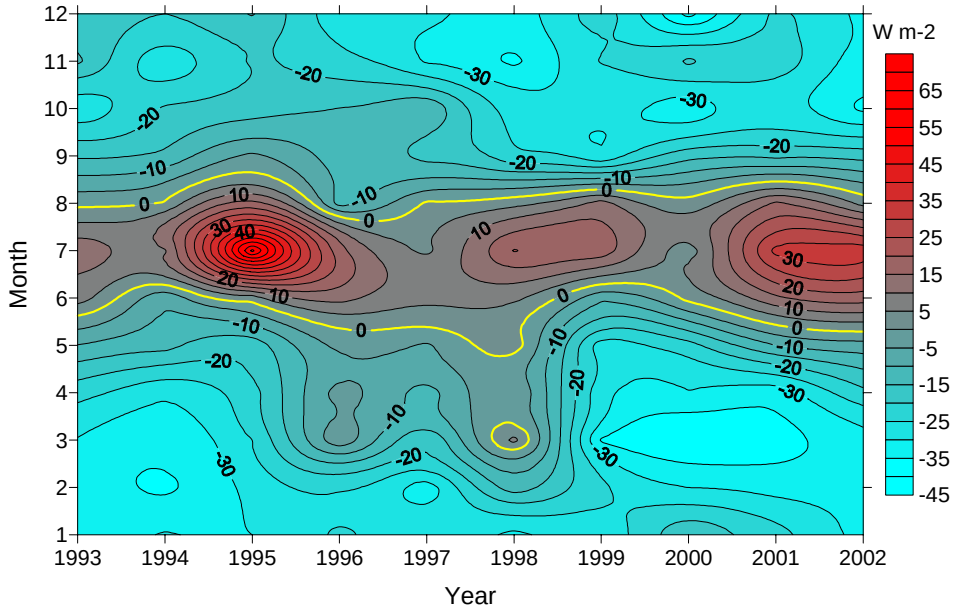

Figure 3.2: Interannual variability of net radiation for the Swiss Camp ETH/CU AWS record from 1993 through 2002.

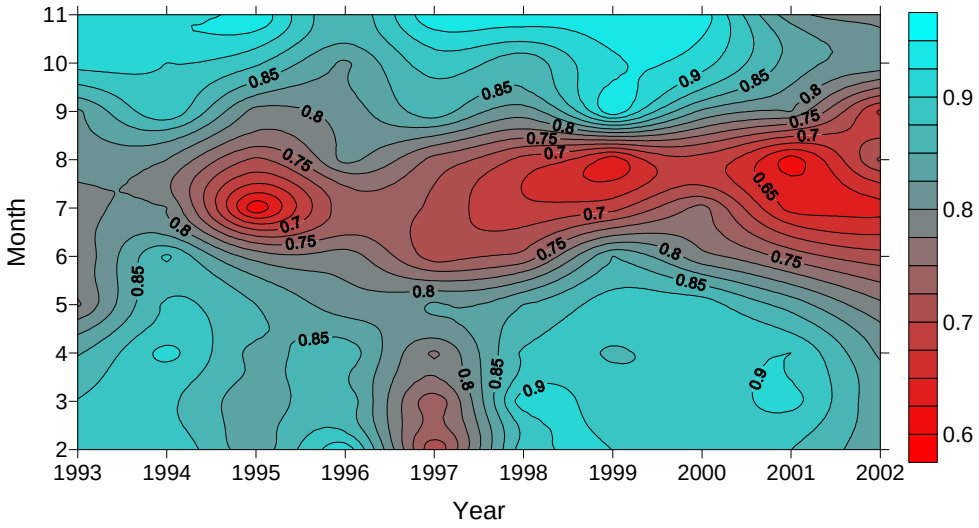

Figure 3. 3: Interannual variability of monthly mean albedo at the Swiss Camp ETH/CU station (1993 – 2002).

It is interesting to note, that during the years with maximum insolation (1993 and 1996), the air temperature (Figure 3.1) and the net radiation did not reveal a significant increase. This demonstrates how sensitive the surface energy balance is to albedo and cloud cover on the ice sheet during summer months. Monthly mean net radiation values at the equilibrium line altitude are only positive during June and July, whereas for the remaining part of the year, the sensible heat flux must compensate for the radiative energy loss by turbulent energy transport from the atmosphere to the surface.

The diurnal cycle of net radiation ranges between –80 W m^{-2} to 130 W m^{-2} for cloud-free days, and again the surface albedo is the major driver for the day to day increase or decrease of radiative fluxes (i.e., at solar noon). An increase in net radiation results when the snow surface starts to melt, whereas increase of drifting snow from higher elevations causes a decrease in net

radiation due to the higher reflectivity of the new snow. The ten-year annual mean net radiation value –13.9 W m^{-2}, and for the winter month November – February a negative mean flux density of –26.4 W m^{-2} was recorded.

3.2 Temperature and Surface Energy Balance at Summit

Ongoing measurements at Summit have enabled a temperature history of central Greenland to be reconstructed dating back to 1987 [*Shuman et al.*, 2001; Box, 2002]. Using records from the GC-Net AWS station these records have been up dated to 2002, which gives a mean annual temperature at Summit of -29.5 °C for the period 1987-2002. Figure 3.4 shows that during that time 1992 was by far the coldest year. An annual increase of temperature of 0.03 °C/yr has occurred during this time but is not statistically significant ($p > 0.05$). Winter temperatures (DJF) have increased by 0.21 °C/yr but this trend is also not statistically significant. Interestingly, over the period 1987-2002 summer temperatures (JJA) have decreased at Summit by 0.16 °C/yr, and is significant at the $p < 0.06$ level. This record is one of the longest time series of temperature on the Greenland ice sheet and is becoming increasingly important to the ongoing snow chemistry studies at Summit.

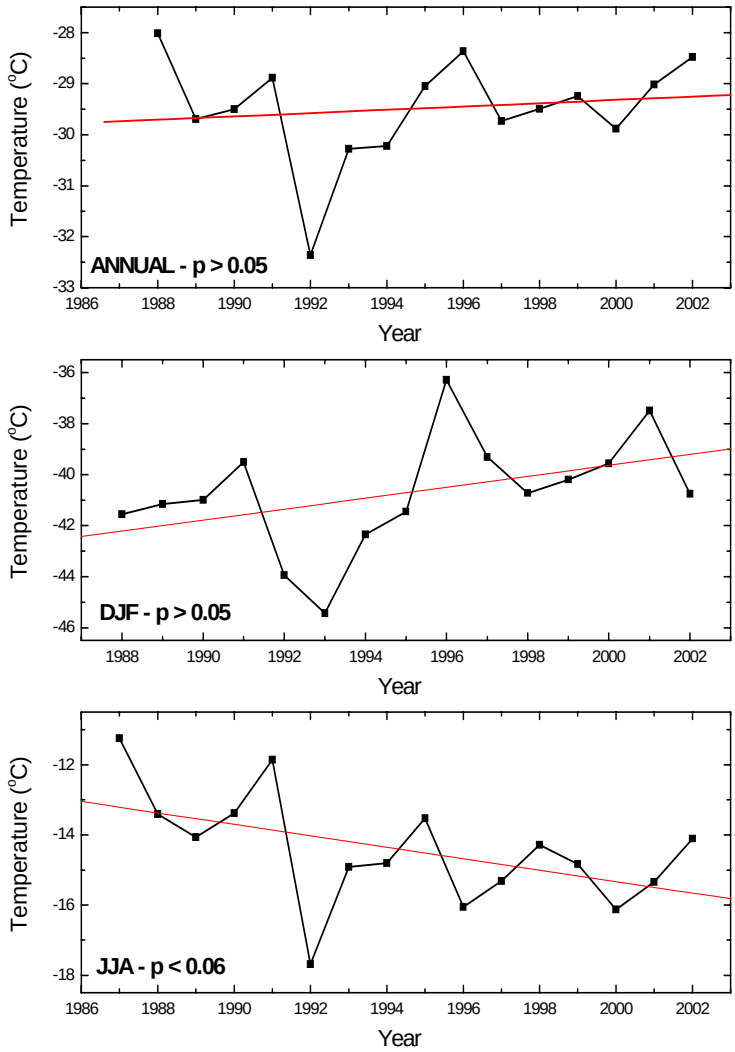

Figure 3.4: Time series of temperature at Summit between 1987-2002 annually (top), winter (middle) and summer (bottom).

In addition to GC-Net measurements made at Summit additional radiation and actively ventilated profile measurements at 3 levels were made on 2 separate towers, respectively, between the summers of 2000-2. The precision radiometry has enabled the 4 main components of the radiation balance to be determined on an annual basis for the first time. To complement the radiation exchanges turbulent fluxes of latent and sensible heat were calculated from the actively ventilated measurements of temperature and humidity, while the ground heat flux was determined using temperature profiles from thermistors in the upper layers of the snow and firn at Summit.

The surface radiation budget in summer is characterized by some of the highest incoming global radiation values in the Northern Hemisphere due to 24-hour sunlight and persistent clear skies (Figure 3.5). However, the impact of global radiation on the energy balance is to a large extent limited because the dry snow at Summit is so reflective, with surface albedo about 0.82 in spring and summer (Table 1). In the absence of sunlight between mid November and early February radiative exchanges are restricted to the thermal region of the electromagnetic spectrum (Figure 3.5). There is no diurnal cycle of long-wave radiation throughout the winter months, with net-all wave radiation (Q*) values at or near –20 W m^{-2}. In contrast, surface outgoing long-wave radiation (Q_{lo}) responds to high insolation in summer and is often considerably warmer than the atmosphere, resulting in larger monthly values of net long-wave radiation (Q_l). This is important as it restricts the effect of increases in net short-wave radiation (Q_s) in summer, with monthly Q^* values never greater than 20 W m^{-2}. The diurnal course of Q_l in summer is in phase with Q_{lo}.

The net all-wave radiation flux is the basic input to the surface energy balance (Figure 3.6). Turbulent fluxes of sensible heat flux (Q_H) account for about 60% of radiative losses (Q^*) during winter, while the latent heat flux (Q_E) and conductive heat flux (Q_G) are very small but also directed towards the surface. The negative heat fluxes (Table 1) reflect the typical stable stratification of the atmosphere in winter. However, Figure 3.6 shows that daily variability of Q^* and Q_H in winter is often large, with the range of both terms over 40 W m^{-2}. As discussed, this most likely reflects an increase in cloud amount and/or wind speed in response to changes in large-scale flow. The lack of atmospheric water vapor for condensation or sublimation is responsible for limiting Q_E through out the winter months. Heat conduction in the snow is also small due to low conductivity and lack of solar heating. More difficult to explain is why the non radiative terms of the energy balance cannot always account for Q^* at the surface. This imbalance is also observed using only eddy correlation derived turbulent fluxes in FS00 [*Cullen and Steffen*, 2001]. However, the annual residual is only 0.45 W m^{-2}, but is larger if the modeled annual Q_G value (-0.11 W m^{-2}) is used. This implies that the turbulent heat fluxes are most likely underestimated.

Daily and monthly values of Q^* are positive between May and August, which results in turbulent fluxes being directed away from the surface (Figure 3.6). The onset of this occurs in May, which coincides with the restructuring of larger-scale circulation near and over Greenland [*Rogers et al.*, 1997]. However, the steady increase in Q^* from negative to positive values starts as soon as the sun reappears after winter (Figure 3.6a), which is a reminder that radiative forcing, in response to Earth-Sun geometry, is the single most important control on the energy balance. The impact of Q_H being directed away from the surface is that it changes the stratification of the near-surface atmosphere from stable to unstable (42% of all cases in JJA). A rise in air temperatures enables the atmosphere to carry more moisture, resulting in small but positive fluxes of Q_E (sublimation from the surface). The magnitude of Q_G is comparable to the turbulent fluxes, and as expected, has a weak cooling effect on the surface during summer. A discrepancy between modeled and calculated values in summer suggests that problems may exist in determining Q_G because of solar heating of thermistors. This may explain in part the residual in Table 1 but does not affect the sign of the flux (into the snow during summer).

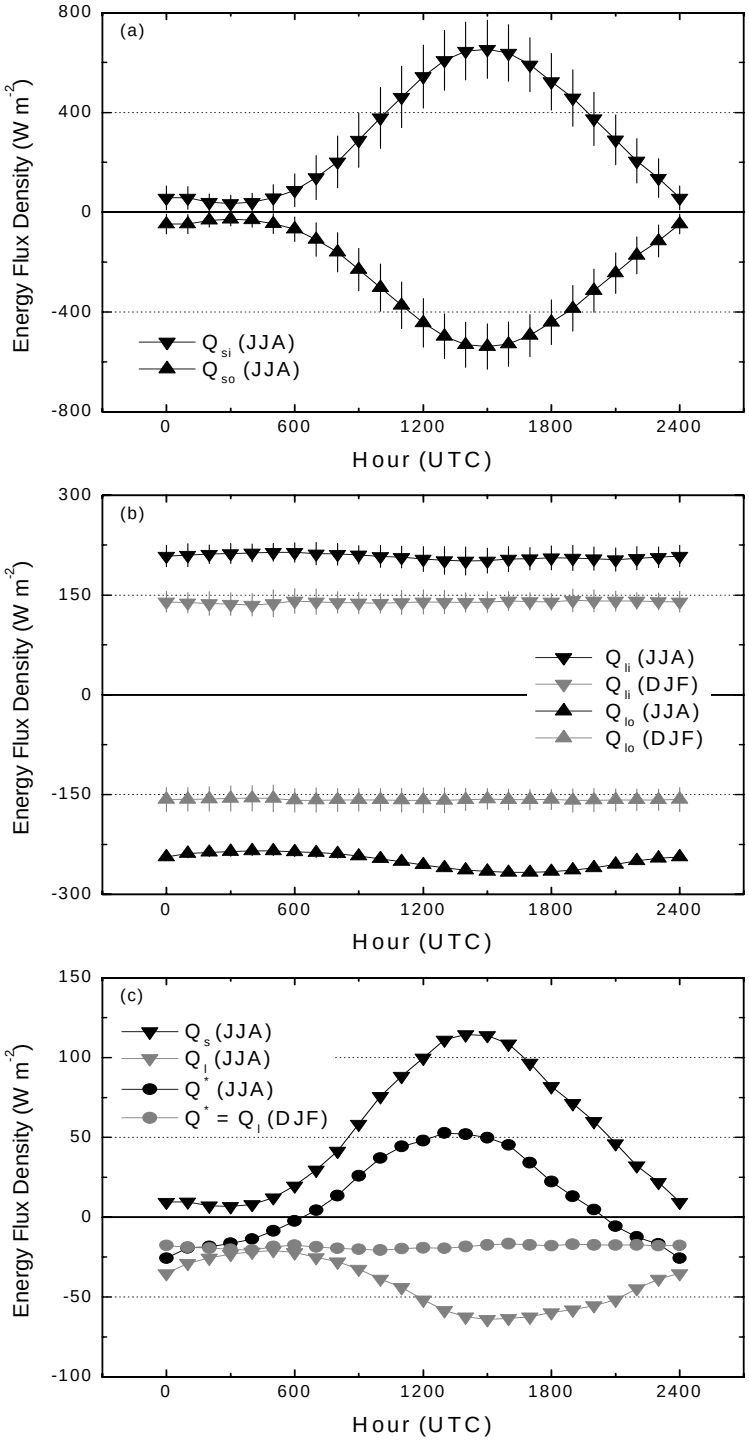

Figure 3.5: Typical diurnal profiles of radiation during summer (JJA) and winter (DJF) for (a) short-wave and (b) long wave and (c) net radiation terms.

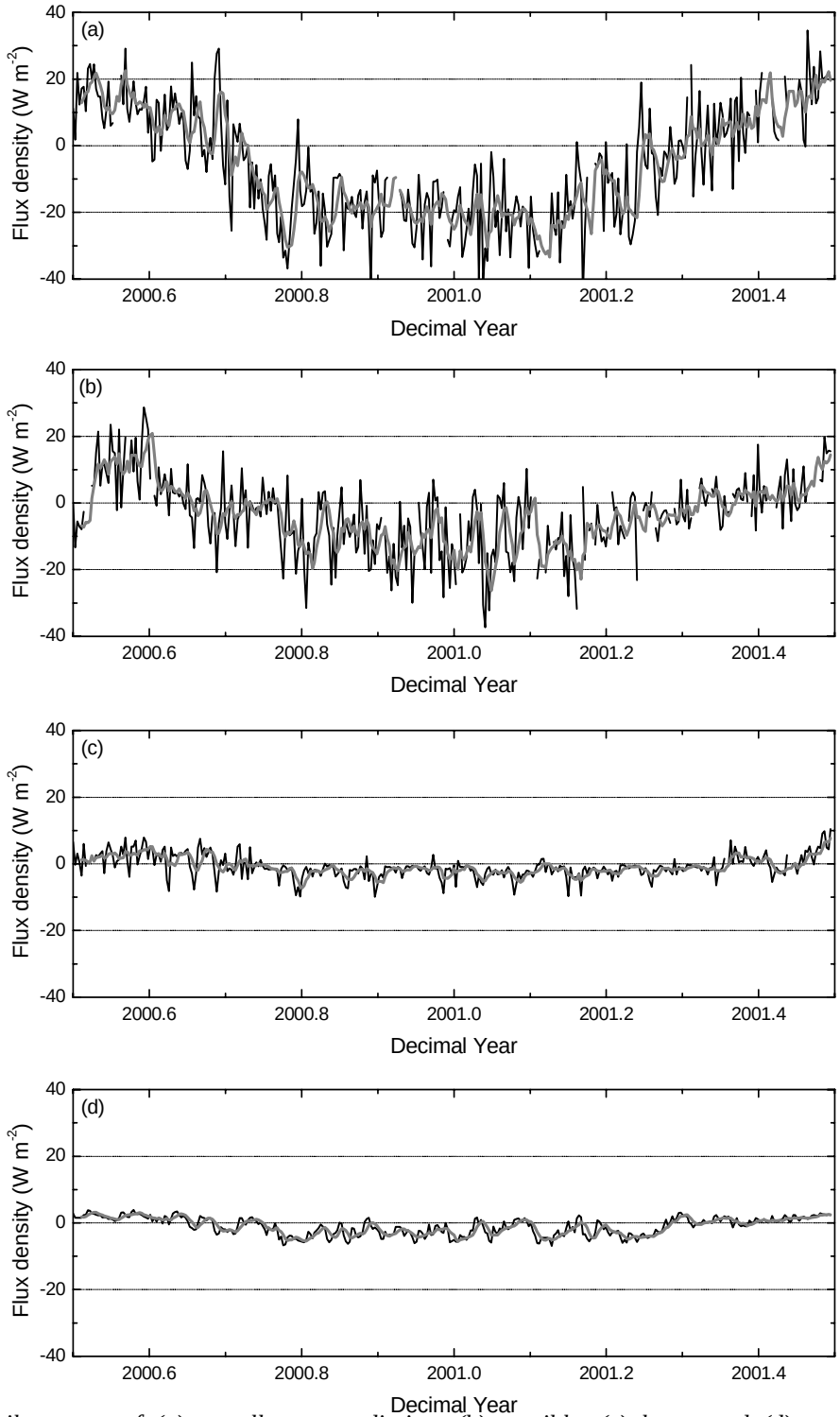

Figure 3.6: Daily means of (a) net-all wave radiation, (b) sensible, (c) latent and (d) conductive (ground) heat fluxes between July 1 2000 and June 30 2001. The solid gray line in each panel shows a 5-point running mean of the energy exchanges.

Table 1: Mean monthly values for all components of the energy balance between July 1 2000 and June 30 2001. Monthly means are only included if 85% of all hourly values are available.

	JUL	AUG	SEP	OCT	NOV	DEC	JAN	FEB	MAR	APR	MAY	JUN	YEAR
Q_{si}	334.7	216.9	103.9	30.9	1.4	0.0	0.2	13.6	96.1	206.9	328.2	392.7	143.78
Q_{so}	274.2	181.5	85.1	24.0	0.9	0.0	0.1	10.8	76.5	169.9	268.4	322.1	117.78
Q_{li}	210.1	224.1	203.7	144.5	151.4	136.5	147.5	141.5	124.1	145.2	158.6	190.7	164.83
Q_{lo}	255.4	251.3	224.4	169.9	169.5	156.6	168.5	166.5	157.0	184.2	211.7	246.2	196.76
Albedo	0.82	0.84	0.82	-	-	-	-	-	-	0.82	0.82	0.82	-
Q_s	60.5	35.4	18.8	6.8	0.5	0.0	0.1	2.9	19.6	37.0	59.8	70.6	26.0
Q_l	-45.3	-27.1	-20.7	-25.4	-18.2	-20.0	-21.0	-25.0	-32.8	-39.0	-53.1	-55.5	-31.93
Q^*	15.2	8.3	-1.9	-18.6	-17.7	-20.0	-20.8	-22.2	-13.3	-2.0	6.6	15.1	-5.93
Q_H	7.9	5.1	-2.0	-7.4	-10.2	-12.1	-12.2	-12.5	-6.5	-2.0	1.5	6.3	-3.68
Q_E	2.5	2.0	0.2	-2.7	-2.9	-1.9	-2.4	-2.2	-2.1	-1.7	0.7	1.6	-0.75
Q_G	2.2	1.2	-0.5	-3.5	-2.8	-3.0	-2.1	-2.6	-3.1	-0.7	0.5	1.6	-1.05
Residual	2.6	-0.1	0.4	-4.9	-1.8	-3.1	-4.2	-4.8	-1.6	2.4	3.9	5.6	-0.45

3.3 Surface Melt Extent in 2003

The surface melt extent for 2003 was processed from the daily gridded brightness temperatures measured from the SSM/I passive microwave satellite. A map of all pixels that experienced melt is presented in Figure 3.7. Figure 3.8 is a plot of the daily melt extents for the 2003 melt season. The 2003 melt season was the fifth largest melt season in terms of total melt and melt extent in the passive microwave record which is continuous since 1979. Figure 3.9 compares the 2003 melt season with the 2002 season which holds the record for maximum melt extent. However, the current passive microwave melt detection algorithms do not capture the intensity of melt on the ice sheet. Figure 3.8 indicates that a very late melt occurred after much of the snow cover had been removed. Also, due to very low precipitation rates on the western flank of the ice sheet, the albedo during the peak of the melt season was unusually low resulting in a highly intense melt season. As a result nearly 1.3 m of ice was melted at the Swiss camp station located near the ELA. Figure 3.10 is a plot of the surface heights measured at the station during the 2003 melt season.

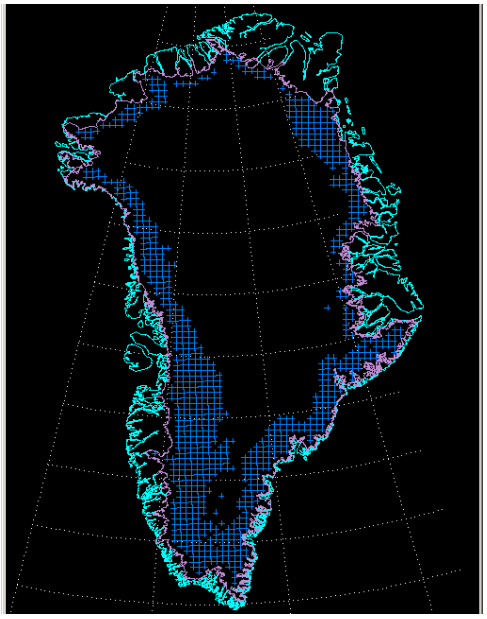

Figure 3.7: Melt extent for 2003 from passive microwave satellite

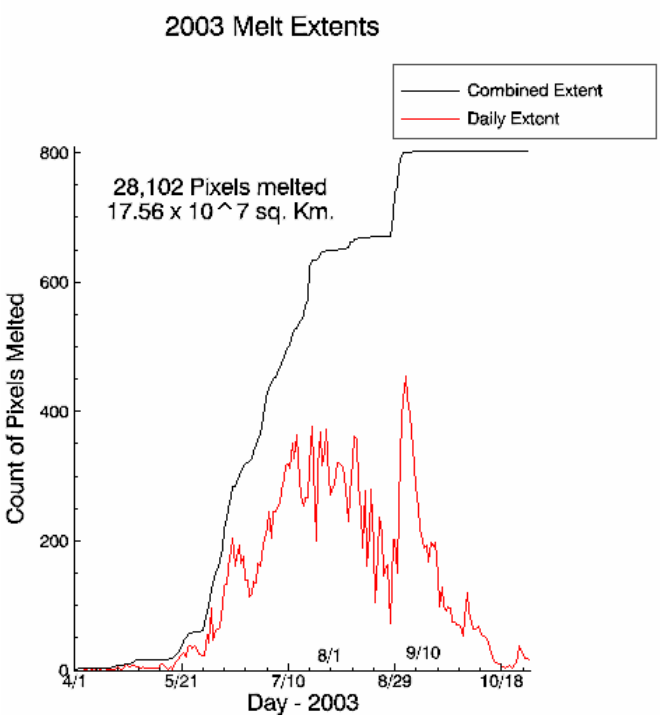

Figure 3.8: Daily melt extent (red) and number of pixels experiencing melt at least once (black) during 2003.

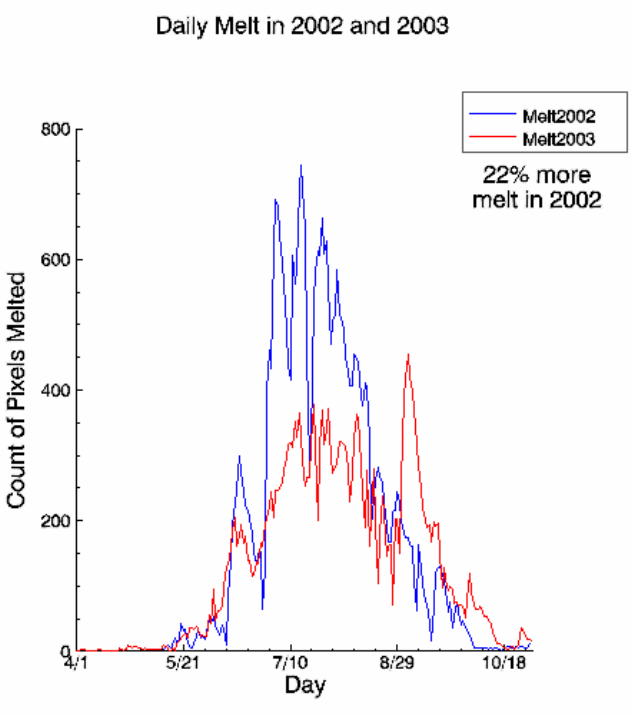

Figure 3.9: Daily melt extent in 2003 compared with the 2002 record year.

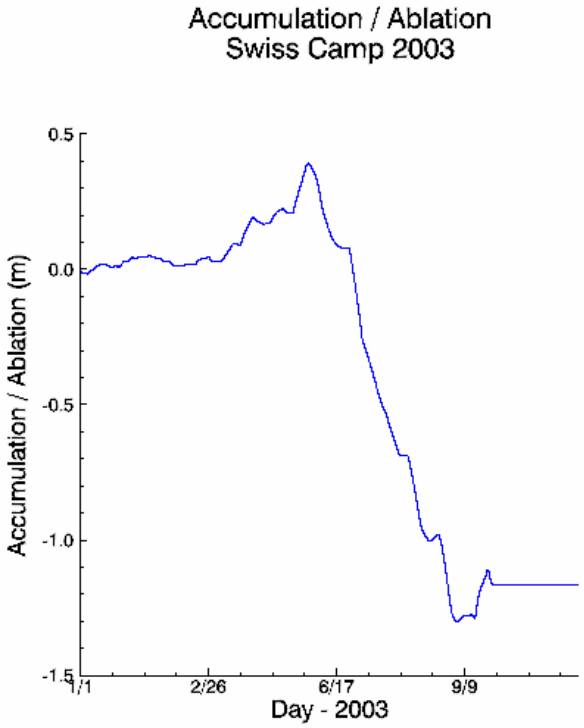

Figure 3.10: Surface height at the Swiss Camp AWS during 2003 indicating melt of 1.3 m of ice near the ELA.

3.4 Cyclone Frequency Distribution

The Arctic is closely monitored for climate change. One indicator of climate change is the frequency of cyclone occurrence. Cyclones are an important mechanism of energy transport from the lower latitudes to the Polar Regions. Any change in frequency will result in a surplus or deficit of energy for that region. Analysis of cyclone frequency in the Arctic over extended periods of time can provide an estimation of present circulation variability and assessment of natural trends. Variations in cyclone frequency can indicate change in the energy distribution of the Arctic Climate System.

Cyclones are a driver of temperature advection and moisture flux for the Arctic. Past studies by Serreze et al. have shown the Atlantic side of the Arctic to be most synoptically active. The current study up to this point has focused on a region bounded by 55°N-90°N and 270°E-360°E and labeled as the Quadrant. The area encompassed by Greenland was avoided due to a pressure reduction problem over the ice sheet. The sector was broken up into 2 sub-regions according to common cyclone paths including areas of formation and dissipation. The Western region includes Baffin Bay/Davis Strait and western Greenland (55°N-90°N, 270°E-315°E). The Eastern region includes eastern Greenland and the Greenland and Barents seas (55°N-90°N, 315°E-360°E). Yearly and seasonal cyclone frequency and intensity, as well as patterns of motion, have been analyzed over the period 1963-2002 and are being compared to a 24-year melt extent record of the Greenland ice sheet derived from passive microwave data.

Cyclone detection was determined using a six-hourly NCEP Reanalysis dataset of gridded sea level pressure provided by the Cooperative Institute for Research in Environmental Science/ National Oceanic and Atmospheric Administration Climate Diagnostics Center. The detection and tracking algorithm was developed by Mark Serreze and Fiona Lo and is based on that used in *Serreze et al.*,[1993] and *Serreze* [1995, 1997]. The algorithm is based on gridded sea level pressure analyses in which each cyclone is identified and given a number that it retains throughout its life. Tracking is based on an 800 km maximum distance of travel per 6-hour time step and a 'nearest neighbor analysis'.

The general directions of cyclones within the Quadrant were east-northeast along the east coast of Greenland and toward the Barents and Kara seas, or north-northeast along the west coast of Greenland by way of Baffin Bay and Davis Straight. Thus far, our analysis has shown that there has been a significant increase (confident at the 0.01 confidence level) in cyclone frequency within the Quadrant (55°N-90°N, 270°E-360°E) during the melt season (May-September) for the period corresponding to the passive microwave derived melt record, 1979-2002. A similar result was found for the Eastern region (55°N-90°N, 315°E-360°E). This is displayed in Table 2. On average, the Western region (55°N-90°N, 270°E-315°E) has a higher annual frequency of cyclones than the Eastern region during the melt season (May-September). However, cyclone frequency has shown a weak correlation to total melt on the Greenland ice sheet for all regions. This is shown in Table 3.

Similar to the frequency of cyclones, the intensity of cyclones has increased significantly (with a confidence at the 0.05 confidence level) within the Quadrant (55°N-90°N, 270°E-360°E) during the melt season (May-September) for the period corresponding to the passive microwave derived melt record, 1979-2002. A similar result was again found for the Eastern region (55°N-90°N, 315°E-360°E). This is displayed in Table 4. Unlike the result for cyclone frequency, on average, the intensity of cyclones is higher in the Eastern region (55°N-90°N, 315°E-360°E) than in the Western region during the melt season (May-September). Cyclone intensity has shown a

stronger correlation to total melt than cyclone frequency on the Greenland ice sheet for all regions. This is displayed in Table 5.

Future work includes comparing cyclone frequency and intensity to particular melt regions on the Greenland ice sheet as defined by Abdalati and Steffen (2001).

Table 2. Trends in Cyclone Frequency During the Melt Season: (May-September)This table displays the value of the slope of the frequency distribution trend line and the % of significance at the 0.01 confidence level.

Region	**Time Period**	**Slope of Trend line**	**% Significance at the 0.01 and 0.05 Confidence Levels**
Quadrant (55°-90°N, 270°-360°E)	1979-2002	0.93	98%
Quadrant (55°-90°N, 270°-360°E)	1992-2002	3.5	99%
West (55°-90°N, 270°-315°E)	1992-2002	2.1	95%
East (55°-90°N, 315°-360°E)	1979-2002	1.0	99%

Table 3. Correlation Coefficients for Cyclone Frequency and Total Melt of the Greenland ice sheet . This table displays the correlation coefficients for cyclone frequency and total melt of the Greenland ice sheet for different regions.

Time Period	**Quadrant** 55°-90°N, 270°-360°E	**West** 55°-90°N, 270°-315°E	**East** 55°-90°N, 315°-360°E
1979-2002	0.098	0.11	-0.1
1979-1991	0.38	0.17	0.61
1992-2002	0.02	0.1	-0.32

Table 4. Trends in Cyclone Intensity During the Melt Season (May-September).This table displays the value of the slope of the intensity distribution trend line and the % of significance at the 0.01 confidence level.

Region	**Time Period**	**Slope of trend line**	**%Significance at the 0.01 and 0.05 Confidence Levels**
Quadrant (55°-90°N, 270°-360°E)	1963-2002	0.026	99.9%
Quadrant (55°-90°N, 270°-360°E)	1979-2002	0.033	97%
Quadrant (55°-90°N, 270°-360°E)	1979-1991	0.078	99%
West (55°-90°N, 270°-315°E**)**	1963-2002	0.052	98%
East (55°-90°N, 270°-315°E)	1963-2002	0.046	99.99%
East (55°-90°N, 270°-315°E)	1979-2002	0.041	96%
East (55°-90°N, 270°-315°E)	1979-1991	0.094	97%

Table 5. Correlation Coefficients for Cyclone Intensity During the Melt Season (May-September) and Total Melt of the Greenland ice sheet. This table displays the correlation coefficients for cyclone intensity and total melt of the Greenland ice sheet for different regions.

Time Period	**Quadrant** 55°-90°N, 270°-360°E	**West** 55°-90°N, 270°-315°E	**East** 55°-90°N, 315°-360°E
1979-2002	0.13	0.37	0.11
1979-1991	0.32	0.60	0.09
1992-2002	0.06	0.40	0.14

3.5 Evaluation of Cloud Frequency at Summit, Greenland

The results of a validation study over Summit Camp, Greenland of the Moderate-resolution Imaging Spectroradiometer (MODIS) Cloud Mask (MOD_35) data product are here presented. The goal of this work is to determine the range of errors to be expected in using this data set to develop a climatology over Greenland's high plateau. It is expected that there will be shortcomings in the MOD_35 product because of the inherent difficulties of high latitude cloud detection [*Key and Barry*, 1989; *Schweiger and Key* 1992; *Schweiger et. al.*, 1999]. It is also important to understand how errors in the MOD_35 will propagate through other data sets and data products. This validation is a single point analysis that will be applied over the dry snow region.

MOD_35 (v.4) was developed at the University of Wisconsin and is now in its fourth version [*Ackerman et. al.*, 1997]. The MOD_35 algorithm relies on a domain description to decide which spectral tests will be used in identifying clouds for a given pixel. Due to the limitations of satellite cloud detection in high latitudes, over snow and ice and at high altitude, fewer tests are applied in this domain over the high plateau of Greenland: 2 during daylight hours; 3 during polar night. Daylight hours are partitioned by a solar zenith angle of less than 85°. Automated snow detection is used during daylight hours based on a Normalized Difference Snow Index (NDSI) algorithm. When this algorithm fails to detect snow/ice over the high plateau of Greenland an additional three tests are run. The results of the validation indicate that failure in the NDSI algorithm typically gives rise to failure in the cloud detection algorithm over Greenland.

The validation approach compares two high-quality, independent, ground-based data sources with MOD_35: a whole sky images and a ceilometer. The validation evaluates a single ensemble pixel (5 km-square) from MOD_35 located over Summit that represents the average of 25 - 1 km resolution cloud mask pixels. During daylight hours, the ground data set is comprised by both the sky camera and ceilometer. During nighttime hours, the ground data set relies on the ceilometer data alone.

After being filtered for confidence and homogeneity, the ground data was grouped into three categories: high confidence clear (<15% cloud cover – zero at nadir), high confidence cloud (>90% cloud cover) and mixed skies (>15% and <90%). The ground data was thus partitioned to convert the linear sky cover percentage data into a similar format to the MOD_35 discrete data. Using the same designation to that of MODIS, high confidence clear is assigned a value of '3' and high confidence cloud is assigned a value of '0' in the ODS.

A conditional probability matrix was compiled from all of the high confidence comparison points. This matrix describes the probability that MOD_35 will have a certain value, given the value of the ODS. The results are partitioned by sky regime according to the ODS: clear or cloudy. The probability matrix converts a binary comparison back into a format from which error ranges can be generated and applied to the climatology. This approach also allows misidentified clear scenes and misidentified cloudy scenes to be separately described and evaluated.

A total of 166 nighttime scenes and 185 daytime scenes qualified for the validation after the filters were applied to ground data. A handful of low confidence results are thrown out of the analysis. Over 95% of all results are high confidence. A sufficient number of examples qualified to generate confident statistics about the behavior of both algorithms during both sky regimes. The results of the initial validation are presented in Table 6, "unfiltered". The unfiltered results show strong deficiencies in spring/fall clear sky detection.

Results indicate that failure in the cloud detection algorithm was frequently related to an angular dependence failure in the NDSI algorithm. The NDSI algorithm does not model the bidirection reflection differencing function (BRDF) of the snow surface. The BRDF of snow surfaces is well described [*Steffen*, 1987], and is known to demonstrate strong forward and backward scattering at certain viewing angles. The cases of successful and failed snow/ice detection

for clear days only were investigated for this angular dependence. The results are present in Figures 3.11 a-d. The ordinate axis is solar zenith angle, the abscissa is the difference between the sensor azimuth and solar azimuth (*dAz*) and the results are grouped by sensor zenith. Failed NDSI results are associated with both positive and negative *dAz.* Those associated with positive *dAz* are more likely to occur at sensor angles less than 45° than those with negative *dAz* at sensor angles greater than 30°. There is a high NDSI failure rate associated with *dAz* between -60° and -70°. This is especially true at high solar zenith angles when sensor zenith is also high. Of the 19 observations that fall in this category, 14 are associated with failed NDSI. This would suggest rejecting MOD_35 clear sky data that falls within this viewing geometry (solar zenith > 55°, sensor zenith > 30°) from the climatology in order to improve confidence in the final results. Steffen (1996) observed surface reflection enhanced by a factor of 1.2 at the angles identified as problematic above (*dAz* ~120°, Solar > 60°, Sensor > 45°) in measurements taken over snow in Greenland.

Table 6. Results of MOD_35 validation: Unfiltered and Filtered.

Data Set	Season	Daytime		Nighttime	
		P(M3|G3)	P(M0|G0)	P(M3|G3)	P(M0|G0)
Unfiltered	Winter	-	-	**0.86**	**0.50**
	Spring	0.38	0.86	**0.86**	**0.42**
	Summer	**0.93**	**0.90**	-	-
	Fall	-	**0.93**	**1.00**	**0.71**
BF 19 Filter	Winter	-	-	**0.86**	**0.50**
	Spring	**0.92**	**0.88**	0.86	0.42
	Summer	**1.00**	**0.70**	-	-
	Fall	-	**0.93**	**1.00**	**0.71**
Angle Filter	Winter	-	-	**0.86**	**0.50**
	Spring	**0.69**	**0.88**	0.86	0.42
	Summer	**1.00**	**0.79**	-	-
	Fall	-	**0.94**	**1.00**	**0.71**

An understanding the role of NDSI in the cloud detection algorithm performance can be useful for filtering the MOD_35 data set. Filtering the data set improves the probability that MOD_35 will correctly identify cloud and clear skies. When NDSI fails, 3 tests are run that are not appropriate over snow/ice surfaces. By re-factoring the final cloud mask determination without these tests, the performance of the algorithm is improved. This is filter is presented in Table 6, "BF 19". This filter dramatically improves springtime clear sky detection, but hurts summertime cloudy sky detection. Another option is to filter out problematic viewing angles. This option yields less improvement in springtime clear sky detection, but not has as negative an affect on summertime cloudy sky detection.

Conclusions: Summit, Greenland is an extreme environment for the performance of any satellite data product. Atmospheric water vapor is very low, surface inversions are common and polar night conditions prevail for half of the year. MOD_35 performs well in this environment in spite of having been optimized for lower latitudes and implementing coarse domain-based thresholds. Its performance over Summit and likely all of Greenland could be improved by the application of more locally appropriate thresholds and specifying snow and ice cover rather than using NDSI.

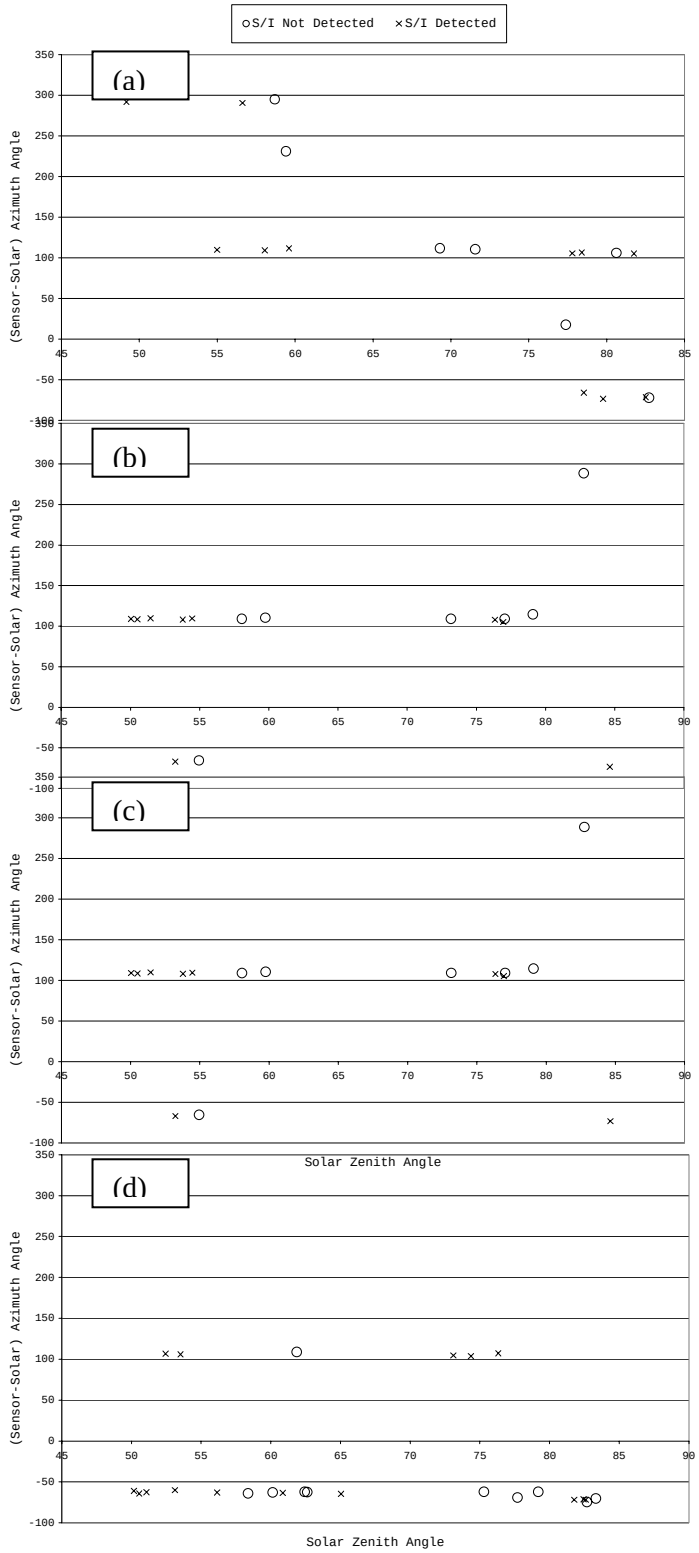

Figure 3.11: Angular Dependence in NDSI Snow and Ice (S/I) Detection and Failures; a. Sensor Zenith < 15°; b. 15° < Sensor Zenith < 30°; c. 30° < Sensor Zenith < 45°;

3.6 Ablation Study in the Jakobshavn Region

An intensive study area has been established in the Jakobshavn ablation region (JAR), west-central Greenland, to conduct a detailed process and modeling study of ablation. A total of three AWS have been installed, collecting data in the ablation zone since mid-1996. In May 2001, four smart stakes (SMS) were installed in the ablation zone to increase the spatial and elevational coverage of the AWS. One year of data has been retrieved from these four SMS, and two additional years of data will be collected in upcoming field seasons.

To help better assess the spatial variability of ablation, the meteorological parameters that control ablation, and the accuracy of interpolating temperatures to similar elevations off of the established transect, a fifth SMS was installed in May 2002. SMS-5 was installed at a similar elevation as SMS-2, but several kilometers to the north in a different basin. The first year of data from SMS-5 will be collected in the upcoming field season due to malfunctioning in the first field season.

A semi-analytical, one-dimensional snow and ice melt model, SOSIM, is presently being developed for the region. The model will used data collected by the AWS and SMS, as well as satellite data and data collected in the field each season to derive ablation over a grid covering the study area. The goal of the model is to derive snow and ice loss at each grid cell (approximately 250 x 250 m^2) in the model to an accuracy of ± 5 cm..

The model is forced with mass and energy fluxes derived from the SMS and AWS data and derives changes in snow depth, snow properties including water content, superimposed ice formation, and ice melt. An early version of the model, which runs at a single point, calculates the total annual ablation to within ± 50 %. This is quite promising since much of the physics that will go into the final model have not yet been included, and, at present, the model is using arbitrary and constant values for snow density, snow depth, snow temperature and ice temperature. Snow temperature and density are measured once per year at each station, while ice temperature is monitored hourly at the AWS and snow depth is measured hourly at the AWS and SMS. Surface height changes recorded at the eight stations (3 AWS and 5 SMS) will be used to validate the model.

Additional studies are planned for the upcoming field season. These include a relative temperature calibration of all eight stations, a study of the spatial variability of air temperature, and a scale study of the topography. The results of these studies will help in the development of SOSIM, and will enable a better estimation of the model uncertainty.

The Pâkitsoq region of west-central Greenland is one of the most intensely monitored portions of the Greenland Ice Sheet, and is the major focus of a recent PARCA initiative. A profile of 11 AWS and SMS has been established along an elevation transect extending from Summit (3254 m a.s.l.) down to JAR3 (323 m a.s.l.) near the margin, creating the largest elevation transect on a glacier in the world. Data from these stations have been supplemented with data from 150 ice core and snow pit locations in the region to create a mass-balance profile along the transect.

The mass balance profile is plotted in Figure 3.12 along with the average annual net accumulation from the PARCA ice cores. Comparing the ice core data with the more recent snow pit and station data suggests a possible steepening of the mass balance gradient through time, which would be expected with a general climatic warming [*Dyurgerov and Dwyer*, 2000], although this will be investigated further.

Annual snow density profiles collected along the transect reveal no coherent pattern in the depth-density relationship for first-year snow (Figure 3.13). This is due to the stochastic nature of snow accumulation and the densification processes occurring throughout the year. The mean density of the snow layer, established through the relationship between snow depth and water-

equivalent snow depth, is nearly constant, both along the transect and from year to year (Figure 3.14).

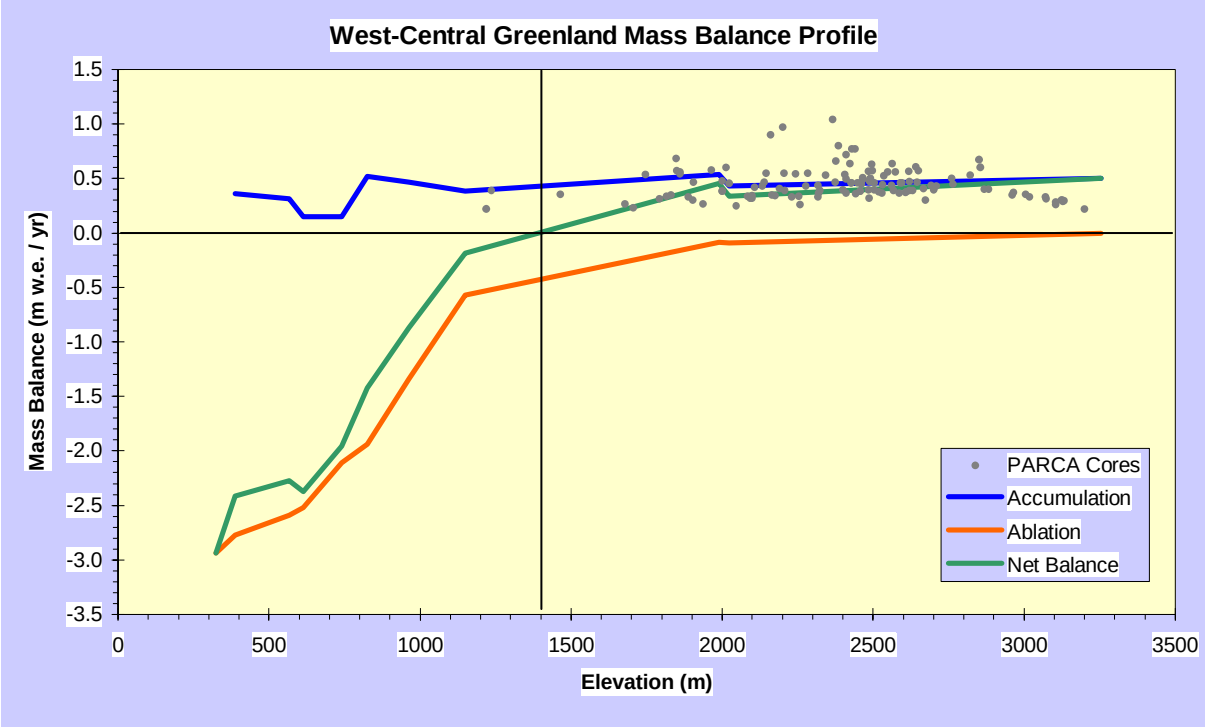

Figure 3.12: Mass balance profile along an elevation transect from Summit, Greenland, to the western margin.

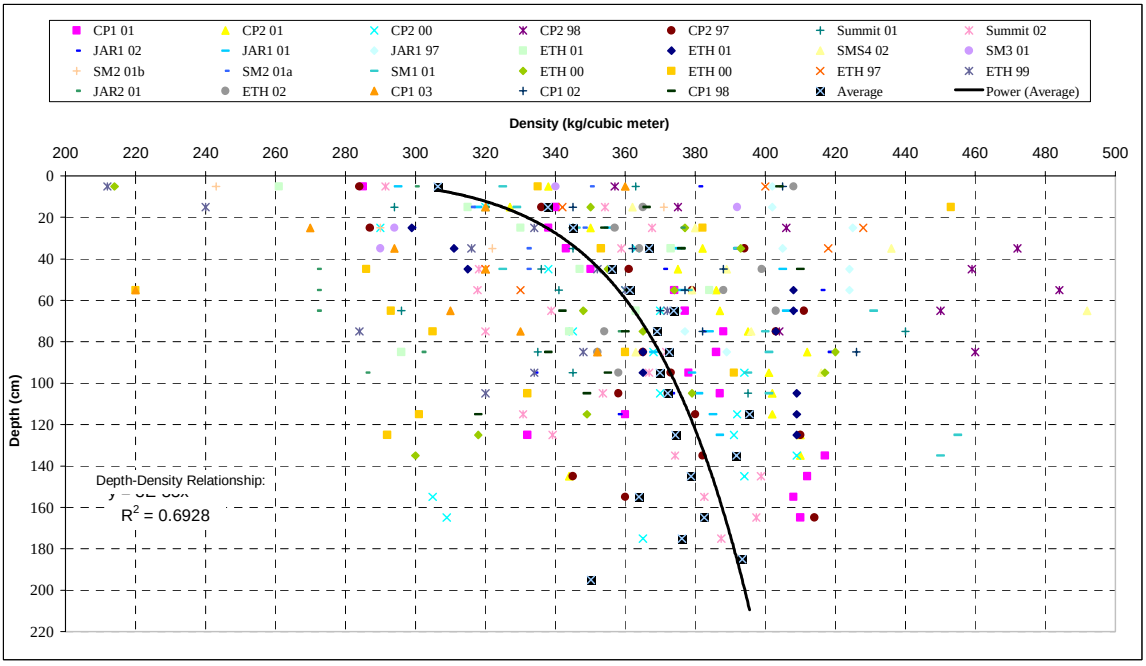

Figure 3.13: Density profiles from snow pits collected between 1997 and 2003.

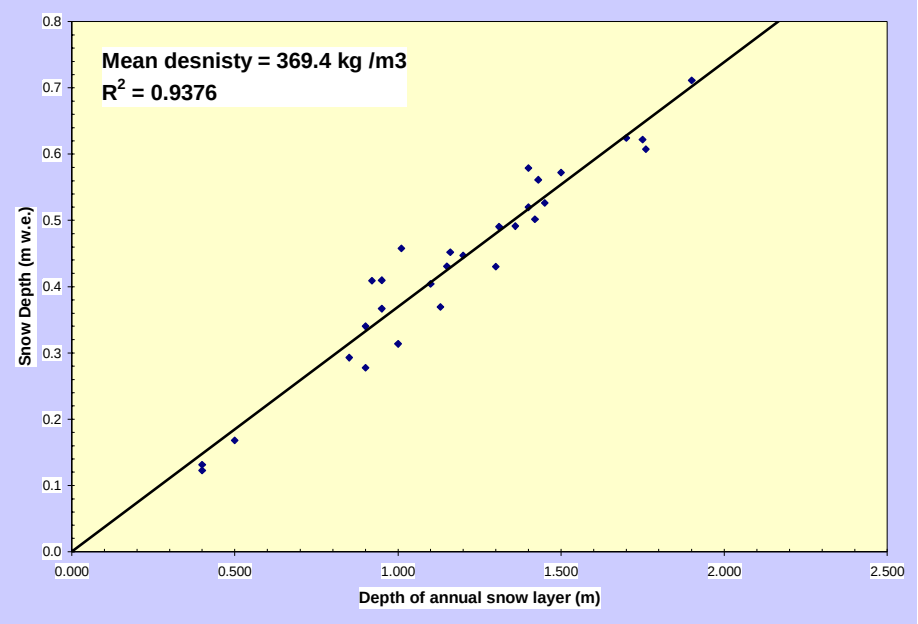

Figure 3.14: Relationship between the depth of the annual snow layer and the water-equivalent depth reveals a consistent mean snow density along the profile and from year to year.

4. PROPOSED FIELD ACTIVITIES AND RESEARCH OBJECTIVES 2003

4.1 AWS Maintenance

The automatic weather station network will be maintained. In the north, the Petermann and Petermann EL stations will be serviced as part of the NSF/NASA supported field activities. The profile JAR3, JAR2, JAR1, CU/ETH, and Crawford 1 will be serviced while at the Swiss Camp. In the southern part of the ice sheet we will service the DYE-2, Saddle, and NASA SE sites (Fig. 1.1) to reactivate the satellite transmitter, download the data and collect snow stratigraphy information. Short visits to Summit and possibly NGRIP are planned.

4.2 Ablation Modeling and Smart Stakes

Our effort to monitor the ablation along a transect from the Swiss Camp to the ice margin will continue. We have installed five "smart stakes" in spring 2001 and 2002, and will service these sites during our AWS support in the ablation region. We will continue to collect high-resolution surface topography data using Trimble Pathfinder differential GPS measurements along several transects in the lower ablation region. In addition, we will acquire a sequence Landsat TM satellite imagery during the onset of melt and melt period to monitor the spatial variation and extent of snow fields in the ablation region.

4.3 Ground Penetration Radar

We have collected a number of ground penetrating radar (GPR) profiles along the western slope of the ice sheet (Jakobshavn and Kangerlussuaq region) in previous field seasons (1999, 2000, 2003). The analysis of this data set showed that the accumulation could vary up to 40% between the trough and the ridge of the undulation. The surface topography with scale length of several kilometers plays an important role for the spatial variability of accumulation, the mass transfer, and the surface energy balance. During the AWS maintenance in the north, we will use GPR to

map the local accumulation variability around the AWS sites, together with snow pit studies (accurate snow density and layer studies). These data will proved further insight to local accumulation retrieved by the sonic height measurements, corrected with a snow densification model.

4.4 NCEP Reanalysis, NAO, and Melt Extent

We will continue the analysis of the surface temperature fields using the NCEP reanalysis and AWS data to compare the present climate with past decades. Further, we will perform a thorough statistical analysis of pressure fields and melt extent to relate to study the forcing mechanism of large-scale synoptic pattern.

5. REFERENCES

Abdalati, W. and K. Steffen, Greenland ice sheet melt extent: 1979-1999, *J. Geophys. Res*., 106(D24), 33,983-33,989, 2001.

Ackerman, S., and K. Strabala, Discriminating clear-sky from cloud with MODIS algorithm theoretical basis document (MOD35). Madison, WI, CIMMS**:** 129, 1997.

Box, J.E., Survey of Greenland instrumental temperature records: 1873-2001. *Int. J. Climatol*., 22, 829-1847, 2002.

Box, J.E. and K. Steffen, Sublimation on the Greenland ice sheet from automated weather station observations, *J. Geophys. Res*., 106(D24), 33,965-33,982, 2001.

Cullen, N.J., and Steffen, K., Unstable near-surface boundary layer conditions in summer on top of the Greenland ice sheet. *Geophys. Res. Lett*., **28**, 4491-4493, 2001.

Key, J. and R. Barry, Cloud cover analysis with Arctic AVHRR data 1. Cloud detection. *J. Geophys Res.* **94**(D15), 18,521 - 18,535, 1989.

Nghiem, S.V., K. Steffen, R. Kwok, and W.Y. Tsai, Diurnal variations of melt regions on the Greenland ice sheet, *J. Glaciol*., 47(159), 539-547, 2001.

Rogers, J.C., Hellstrom, R.A., Mosley-Thompson, E., and Wang, C.C., An abrupt spring air temperature rise over the Greenland ice cap. *J. Geophys. Res*., **102**, (D12) 13793-13800, 1997.

Shuman, C., K. Steffen, J. Box, and C. Stearn, A dozen years of temperature observations at the Summit: Central Greenland automatic weather stations 1987-1999, *J. Appl. Meteorol*., 40(4),741-752, 2001.

Schweiger, A. and J. Key, Arctic cloudiness: Comparison of ISCCP-C2 and Nimbus-7 Satellite-derived cloud products with a surface-based cloud climatology, *J.Climate* **5**: 1514-1530, 1992.

Schweiger, A., and R. Lindsay, Arctic clouds in multiyear satellite data sets, *Geophys. Res. Lett.* **26**(13), 1845-1848, 1999.

Serreze, M. C., Climatological Aspects of Cyclone Development and Decay in the Arctic, *Atmosphere-Ocean*, vol. 33 (1), 1-23, 1995.

Serreze, M. C., J. E. Box, R. G. Barry, and J. E. Walsh, Characteristics of Arctic Synoptic Activity, 1952-1989, *Meteorology and Atmospheric Physics,* vol. 51,147-164, 1993.

Serreze, M. C., F. Carse, R. G. Barry, and J. c. Rogers, Icelandic Low Cyclone Activity: Climatological Features, Linkages with the NAO, and Relationships with Recent Changes in the Northern Hemisphere Circulation, *Journal of Climate*, vol. 10, 453-464, 1997.

Shuman, C.A., Steffen, K., Box, J.E., Stearns, C.R., A dozen years of temperature observations at the summit: central Greenland automatic weather stations 1987-1999. *J. Appl. Met*., **40** (4), 741-752, 2001.

Steffen, K., Bidirectional reflectance of snow at 500-600 nm. Large Scale Effects on Seasonal Snow Cover. B. G. e. al. Wallington, England, IAHS. **166,** 415-425, 1987.

Steffen, K., Effect of Solar Zenith Angle on Snow Anistropic Reflectance. International Radiation Symposium, Fairbanks, AK, A. Deepak Publishing, 1996.

Steffen, K., and J.E. Box, Surface climatology of the Greenland ice sheet: Greenland climate network 1995-1999, *J. Geophys. Res*., 106(D24), 33,951-33,964, 2001.

6. PUBLICATIONS AND PRESENTATIONS SUPPORTED BY THE GRANT

Abdalati, W. and K. Steffen, Greenland ice sheet melt extent: 1979-1999, *J. Geophys. Res*., 106(D24), 33,983-33,989, 2001.

Box, J.E. and K. Steffen, Sublimation on the Greenland ice sheet from automated weather station observations, *J. Geophys. Res*., 106(D24), 33,965-33,982, 2001.

Bromwhich, D., J. Cassano, T. Klein, G. Heinemann, K. Hines, K. Steffen and J. Box, Mesoscale modeling of katabatic winds over Greenland with Polar MM5, *Mon. Weather Review*, 129, 2290-2309, 2001.

Cassano, J.J., J.E. Box, D.H. Bromwich, L. Li, and K. Steffen, Evaluation of Polar MM5 simulations of Greenland's atmospheric circulation, *J. Geophys. Res*., 106(D24), 33,867-33,890, 2001.

Cullen, N., and K. Steffen, Unstable near-surface boundary conditions in summer on top of the Greenland ice sheet., *Geophys. Res. Lett*., 28(23), 4491-4494, 2001.

Jacobi, H.W., M.M. Fey, M.A. Hutterli, R.C. Bales, N.J. Cullen, K. Steffen and C. Koehler, Long-term measurements of hydrogen peroxide and formaldehyde exchange between the atmosphere and surface snow at Summit, Greenland, *Atm. Environm.*, 36, 2619-2628, 2002.

Helmig, D, J. Boulter, D. David, J. Birk, N. Cullen, K. Steffen, B. Johsnon, S. Oltmans, Ozone and meteorological boundary-layer conditions at Summit, Greenland, *Atm. Environm.*, 36, 2595-2608, 2002.

Honrath, R.E. Y.Y. Lu, M.C. Peterson, J.E. Dibb, M.A. Arseault, N.J. Cullen, and K. Steffen. vertical fluxes of NOx, HONO, and HNO3 above the snowpack at Summit, Greenland. *Atm. Environm*, 36, 2629-2640, 2002.

Nghiem, S.V., K. Steffen, R. Kwok, and W.Y. Tsai, Diurnal variations of melt regions on the Greenland ice sheet, *J. Glaciol*., 47(159), 539-547, 2001.

Smith, L.C., Y. Sheng, R.R. Foster, K. Steffen, K.E. Frey, and D.E. Alsdorf, Melting of small Arctic ice caps observed from ERS scatterometer time series, Geophys. Res. Lett., 30(20), CRY 2-14, 2003.

Steffen, K., and J.E. Box, Surface climatology of the Greenland ice sheet: Greenland climate network 1995-1999, *J. Geophys. Res*., 106(D24), 33,951-33,964, 2001.

Shuman, C., K. Steffen, J. Box, and C. Stearn, A dozen years of temperature observations at the Summit: Central Greenland automatic weather stations 1987-1999, *J. Appl. Meteorol*., 40(4),741-752, 2001.

Zwally, H.J. W. Abdalati, T. Herring, K. Larsen, J. Saba, and K. Steffen. Surface melt-induced acceleration of Greenland ice-sheet flow, *Science*, 297, 218-222, 2002.

7. BUDGET

CU Proposal No.

PROPOSED BUDGET DETAILS

Institution: The Regents of the
University of Colorado
572 UCB
Boulder, CO 80309-0572

Title: Variability and Forcing of Climatic Parameters on the Greenland Ice Sheet: Greenland Climate Network (GC-Net)
NASA Awd No. NAG5-10857

Principal Investigator: Konrad Steffen

Duration: 5/1/04 - 4/30/05

	Year 4
A. Salaries and Wages	
Principal Investigator: Konrad Steffen	
100% time, 2 months summer	25,555
100% time, 4 months (Sabbatical)	51,110
Graduate Research Assistant: TBD	
75% time, 3 mos. summer	6,565
50% time, 9 mos. AY	13,242
Undergraduate Research Assistants	
Hourly basis: 450 hrs @ $9.00/hr.	4,050
Total Salaries and Wages	100,522
B. Fringe Benefits	
PI: 21.2% of salary	16,253
GRA: 3.2% of salary	634
Undergraduates: 2.2% of wages	89
Total Fringe Benefits	16,976
Total S/W and Fringe Benefits	117,498
C. Permanent Equipment	
AWS system upgrades	5,150
D. Travel	
Domestic:	
Project personnel to attend scientific conferences (e.g., AGU)-- RT coach airfare: $650 Meals and lodging: $150/day x 4 days Registration fee: $225 Ground transportation: $135	
2 trips/year x $1,610	3,220

	Year 4
Travel continued	
PI to attend PoDAG and IWG meetings--	
RT coach airfare: Denver-Washington, D.C. $550	
Meals and lodging: $150/day x 3 days	
Ground transportation: $100	
1 trip/year x $1,065	1,100
Subtotal Domestic Travel	4,320
Foreign:	
PI travel to attend international scientific conf.	
RT coach airfare: $850	
Meals and lodging: $205/day x 5 days	
Registration fee: $300	
Ground transportation: $200	
1 trip/year x $2,375	2,375
PI Travel to Greenland coordination meetings in Switzerland and Denmark	
RT coach airfare: $1,150	
Meals and lodging: $225/day x 7 days	
Ground transportation: $200	
1 trip in year 4 x $2,925	2,925
Foreign Field Travel to Greenland:	
Three people, one trip each year	
RT coach airfares Denver-Toronto-Ottawa -Sonderstromfiord $1,200, Lodging and per diem	
$200/day x 3 days	5,400
RT coach airfares: Sonderstromfiord-Jakobshavn $350 x 3	1,050
Lodging & per diem prior and post expedition:	
Sonderstromfiord (3 days), Jakobshavn	
(3 days)--3 persons x 6 days x $200/day	3,600
Meal allowance during expedition:	
3 persons x 30 days x $21/day	1,890
Subtotal Foreign Travel	17,240
Total Travel	21,560
E. Other Direct Costs	
1) Materials and Supplies:	
ARGOS Satellite transmission costs	9,370
GOES satellite transmission (at no-cost for this project, 12 stations)	
Office and computer-related supplies	386
Software/ data storage media	850
Photographic products	250
Total Materials and Supplies	10,856

	Year 4
Other Direct Costs continued	
2) Publication Costs	1,650
3) Field Support Services:	
Greenland Air subaward	
Twin Otter costs $1,975/hr x 12 hrs	23,700
Helicopter Flight time $1,785/hr x 7.5 hrs	13,388
Airport fee's and passenger tax	3,000
Subtotal Greenland Air	40,088
Equipment Transport (5,000 lbs.)	
Denver-Greenland-Denver, 1 trip/yr.	5,500
Total Field Support Services	45,588
4) Other Costs:	
Sun workstation maintenance	1,620
Tuition remission (1 resident)	4,660
Telephone tolls, FAX, duplication costs	1,557
Total Other Costs	7,837
Total Other Direct Costs	65,931
F. Total Direct Costs	210,139
G. Indirect Costs	
On Campus Research:	
47.4% of MTDC predetermined for the period 7/1/99-6/30/02. 47% of MTDC provisional for the period 7/1/02-6/30/03 and thereafter, per HHS agreement dated 8/16/99.	72,728
Total Indirect Costs	72,728
H. Total Costs	282,867
Total amount requested from NASA for year four:	**$282,867**